Abstract

The processing and characterization of biodegradable nanocomposites based on poly(ester-urethane)s reinforced with different amounts (0.5, 1 and 3 wt %) of nanosized hydroxyapatite (nHA) are reported. The selected poly(ester-urethane) was synthesized starting from a tri-block copolymer based on poly(ε-caprolactone) (PCL) and poly(L-lactic acid) (PLLA). The nanocomposites were prepared by extrusion and by press molding. Several techniques were applied to investigate the properties of the nanocomposites. Electron microscopy revealed that the poly(ester-urethane) matrix is able to phase separate and that the addition of well-dispersed nanofillers modifies the dimension of the segregated phase. The thermal stability of the PU matrix, regulated by the PLLA block, decreased when low contents of nHA (0.5 and 1 wt %) were added, even if the thermal stability of the PCL-block was increased for each nHA amount. The good mechanical response of the nanocomposites confirmed the absence of agglomerates in the dispersion of the nanofillers in the polymeric matrix. The nHA presence also increased the surface hydrophilicity. Furthermore, rheology measurements, mechanical and thermal tests demonstrated the different behavior induced by the addition of nHA in different amounts. In fact, nHA acts as plasticizer at low concentrations (0.5, 1 wt %) and as reinforcement at a higher nHA amount (3 wt %). In vitro degradation tests were performed using a phosphate buffer solution. The results reported here are relevant for the development of nanocomposites based on a biodegradable and biocompatible polymeric matrix reinforced with small amounts of biocompatible nanofillers for different applications, especially in the biomedical field.

Keywords: mechanical properties; phase morphology; nanocomposite; poly(lactide); biodegradable; poly(ester-urethane)

Abbreviations

DMA: Dynamic-mechanical analysis; DSC: Differential scanning calorimetry; FE-SEM: Field emission electron microscopy; HA: Hydroxyapatite; HDI: hexamethylene diisocyanate; nHA: Nanosized hydroxyapatite; PU: poly(ester-urethane); PU+0.5 HA: Nanocomposite of poly(ester-urethane) with 0.5 wt % of HA; PU+1 HA: Nanocomposite of poly(ester-urethane) with 1 wt % of HA; PU+3 HA: Nanocomposite of poly(ester-urethane) with 3 wt % of HA; PCL: Poly(ε-caprolactone); PLLA: Poly(L-lactic acid); TEM: Transmission electron microscopy; T_g: Glass transition temperature;

TGA: Thermogravimetric analysis; T_m: melting temperature; WCA: water contact angle.

1. Introduction

In the last two decades, nanocomposite materials formed by a polymeric matrix and nanofillers from different sources have gained attention of researchers and companies in order to exploit their synergic integration providing new multifunctional properties for different applications [1-3]. Nowadays, the use of polymer matrix nanocomposites is extended to several advanced industrial sectors, from aerospace to automotive, electronics or packaging [4-9]. Indeed, more recently, due to the increase of life expectancy, big efforts have been paid to the developments of new multifunctional nanomaterials for biomedical applications, such as coronary stents, orthopedic devices, wires or scaffolds for bone regeneration [10-13]. Therefore, for these applications both the polymer matrix and the nanofillers must be biocompatible.

In this context, aliphatic polyesters, such as poly(L-lactic acid) (PLLA) and poly(ε-caprolactone) (PCL) represent a good choice for biomedical applications [14-17]. Both biopolymers show different mechanical and thermal properties, allowing to exploit their versatile combination to obtain a material with the desired properties for specific applications. Thus, they can be copolymerized or blended to take advantage of their synergistic combination [18, 19]. Moreover, these polyesters can also be used to design and to synthesize poly(ester-urethane)s by their polycondensation with an isocyanate [20]. Polyurethanes in general, and more specifically, poly(ester-urethane)s, have been already successfully used for biomedical applications due to the possibilities to easily tailor their structure and final properties through a designed synthesis [21, 22].

On the other hand, different nanofillers can be used in biomedicine in order to enhance the properties of the pristine materials [15, 23, 24]. In particular, special interest has been devoted to nanocomposites reinforced with hydroxyapatite (HA) being this material the most relevant mineral component of human hard tissues [15, 25, 26]. However, HA have traditionally exhibited poor mechanical performance, which has restricted their use in many applications [27]. Hydroxyapatite can be modified to achieve nanosized hydroxyapatite (nHA), thus increasing the surface/volume ratio to improve the final properties [28]. The benefits of adding HA nanoparticles to polyester matrices have been widely reported. Kim studied the reinforcement effect of nanosized HA into a PCL matrix finding that it is possible to reach a better dispersion and hence better mechanical properties by using a surfactant [29].

The use of HA, both micro and nanofillers, as reinforcement for polyurethane matrix as well as to promote the cell growth, has been studied previously by different authors [28, 30]. Polyurethane/HA composites are employed to develop new scaffolds, for the cell growth. Dong et al. in fact, reinforced a PU matrix with 10 wt % HA. Even if they observed a decrease in the mechanical properties with the HA addition, they obtained very good results for the cell growth [31]. Laschke et al. demonstrated the possibility to design scaffolds based on poly(ester-urethane) of PCL, 1,4,3,6-dianhydro-D-sorbitol and hexamethylene diisocyanate (HDI) reinforced with 20 wt % nanosized hydroxyapatite, testing the protein adsorption and their biocompatibility [28]. Machado et al. studied the rheological behavior of different composites using polyurethanes as polymer matrices and microsized hydroxyapatite as reinforcement [30]. They used large amounts of HA, 30, 50 and 70 wt % to obtain their composites by extrusion. Also it is important to note that nHA has been used as reinforcement for polyester and polyurethane fibers obtained by electrospinning, incorporating high amounts of nanoparticles in the fibers [32-34].

It is expected that nanocomposites based on nHA will have a better bioactivity than composites based on HA due to the grater surface area which should increase the surface hydrophilicity.Thus, nHA based nanocomposites should promote better adherence of proteins, cell attachment and differentiation of histiocytes [31].

In this work, the processing and characterization of biodegradable nanocomposites using a polymeric matrix based on poly(ester-urethane) reinforced with small amount of nanosized HA are comprehensively studied and reported. The selected polymeric matrix is a poly(ester-urethane) based on a PCL and PLLA tri-block copolymer structure. The nanocomposites were prepared by extrusion and press molding processes by adding different nHA amounts in small contents. Compared with the values reported in the literature mentioned above, we selected low amounts of nanofillers (0.5, 1 and 3 wt %) in order to well understand the effects induced by the nHA. Throughout the paper, the thermal, mechanical, rheological, dynamic-mechanical behavior, surface polarity and the in vitro degradation tests of the biodegradable nanocomposites are studied and related to their morphologies, demonstrating how the addition of different small amounts of nHA affects the properties of the neat matrix and makes these biodegradable nanocomposites attractive for further potential applications in the biomedical field.

2. Materials and methods

2.1. Materials

L-Lactide, HDI, stannous octoate and solvents were purchased from Sigma Aldrich (Spain). PCL diol (CAPA 2403) with a nominal molecular weight of 4000 g/mol was kindly donated by Perstorp (Sweden). A non-commercial hydroxyapatite nanofiller (nHA), synthesized by chemical precipitation method and with particle size of about 35 nm was used [34].

The poly(ester-urethane) (PU) based on PCL and PLLA tri-block copolymer structure, with a ratio of 50:50 between the two blocks, has been synthesized by us in two steps. In the first step the synthesis of the PLLA-PCL-PLLA tri-block copolymer by the ring opening polymerization of L-Lactide started by PCL diol was obtained. The ratio of PCL diol:L-Lactide was 50:50. Stannous octoate was added in 0.1 wt % respect to the L-Lactide monomer. The reaction in bulk at 180 ºC for 3h was carried out. After that, the mixture was dissolved in chloroform and precipitated in cold methanol. The white precipitate was filtered off and dried under vacuum to remove all residual solvents as well as the catalyst.

The molecular weight was calculated by proton nuclear magnetic resonance, giving a value of 7570 g/mol, by comparing the signals of protons of PCL and PLLA as it has been already reported by us elsewhere [20].

The second step was a polycondensation reaction of the obtained tri-block copolymer with the hexamethylene diisocyanate at 1:1 molar ratio. The reaction was performed using dichloroethane as solvent and 0.1 wt % of stannous octoate as catalyst, at 80 ºC for 5h. The initial molar concentration of the tri-blocks was around 0.1 mol^{-1}. After that, chloroform was added to dilute the product and the solution was casted onto a leveled glass. The films were dried under high vacuum. The molecular weight of the polyurethane, of 45,300 g mol^{-1} with a polydispersity index of 1.7, was determined by gel permeation chromatography. More synthesis details are reported previously by us [22].

This poly(ester-urethane) was used as polymer matrix for all the processed nanocomposites.

2.2. Nanocomposites preparation.

Three different compositions, 0.5, 1 and 3 wt % HA with respect to the polymeric matrix were selected, namely PU+0.5% HA, PU+1.0% HA and PU+3% HA, respectively. First, the materials were dried in a vacuum oven at 40 °C during 24 h. After weighting, the materials were manually pre-mixed and added into the extruder. 8 gr of materials were used during each extrusion. All the materials were processed in a DSM Xplore co-rotating extruder at a screw speed of 100 rpm during 3 minutes. The selected temperature profile for the extrusion processing was 145 ºC, 155 ºC and 165 ºC. After the extrusion process, the material was compressed into films of about 500 micron in a Dr. Collin 200mm x 200mm press at 160 °C. There, the samples were heated during 1 min at atmospheric pressure and then 50 bar of pressure were applied during 1 min. The obtained films were cooled to room temperature with water-refrigerated aluminum plates at 50 bar.

2.3. Characterization techniques.

The nanocomposites morphology was analyzed by Field Emission Scanning Electron Microscopy (FE-SEM Supra 25, Zeiss). The films were immersed in liquid N_2 and then fractured. All the samples were gold coated by an Agar automatic sputter coater. The dispersion of nHA into the nanocomposites was studied by Transmission Electronic Microscopy (TEM). TEM measurements were performed on a JEOL JEM- 2100 TEM instrument (JEOL Ltd., Akishima, Tokyo, Japan), with LaB_6 filament and with an operating voltage of 200 kV. The samples were prepared by cryo-ultramicrotomy (LEICA EM UC6) at -90 ºC. Then the samples were put directly onto a 200-mesh cooper grid.

Thermogravimetric analysis (TGA) was carried out using a TA-TGA Q500 analyzer. The experiments were performed using about 10 milligrams of sample from room temperature to 700 ºC at 10 ºC/min under nitrogen atmosphere with a flow of 60 ml/min. The calculated onset temperature corresponds to the temperature of 5 wt % loss of the sample.

Differential scanning calorimetry (DSC) analysis was performed in a Mettler Toledo DSC822e instrument. Samples of about 10 mg were sealed in aluminum pans. A first thermal cycle was performed (from 25 ºC to 200 ºC). After that, a cooling scan from (200 ºC to -90 ºC) was applied to investigate the glass transition temperature (T_g) and the crystallization temperatures (T_c). Finally, a second heating scan was performed (-90

ºC to 200 ºC). All the scans were performed at the same heating/cooling rate of 10 ºC min^{-1} under nitrogen purge. The values of the melting temperature (T_m) were obtained as the maximum of the endothermic peak and the enthalpy of melting (ΔH_m) was calculated as the area below the peaks. The crystallinity of each block of the poly(ester-urethane) was calculated following Eq. 1, where X^a is the fraction of the component a, ΔH_{m0} is the enthalpy for a 100% crystalline material, that is for PLLA was 93 $KJmol^{-1}$ while for PCL was 148 KJ mol^{-1} [22].

$$3_c^a = \frac{1}{1-X^a}\left[\frac{6K_m}{6K_{mO}}\right] \times 100 \qquad \text{Eq. 1}$$

The rheological measurements were performed using a TA Instruments Advanced Rheometer AR1000 with 25 mm diameter stainless-steel parallel plates. The gap was fixed to 0.5 mm. Continuous flow experiments were recorded varying the shear rate from 0.01 to 100 Hz at different selected temperatures.

Dynamic-mechanical analysis was performed in a Mettler Toledo 861e instrument at 1 Hz frequency in tensile configuration. The loss factor (tan δ), the storage modulus (E′) and the loss modulus (E″) were measured from -80 to 80 °C at 10 ºC/min.

Tensile properties were measured in an Instron testing machine equipped with a 100 N load cell. Type 3 dumbbell test specimens (according to ISO 37) were cut from the films. A crosshead speed of 200 mm min^{-1} was programmed. Strain was measured from crosshead separation and referred to the 10 mm initial length. 5 different samples were tested and the average values are reported.

The surface wettability was conducted at room temperature by means of a static water contact angle measurements with a standard goniometer (EasyDrop-FM140, KRÜSS GmbH, Hamburg, Germany) equipped with a camera and Drop Shape Analysis (SW21; DSA1) software was used to test the water contact angle (æº). The contact angle was determined by randomly putting drops of distilled water (=2 µ L) with a syringe onto the PU and PU nanocomposites surfaces and, after 30 s, the average value of ten contact angle measurements for each drop was used. The maximum standard deviation in the water contact angle (WCA) measurements did not exceed ± 3% [35].

The in vitro hydrolytic degradation was performed by immersing the samples under physiological conditions at 37 ºC and pH around 7.2-7.4, using a phosphate buffer

solution (PBS). Each sample was immersed in a vial of 15 ml, filled with 10 ml of solution. The PBS was changed once a week and the pH was checked after each week. Samples were recovered from the buffered solution at different times (one per month during 5 months), rinsed with distilled water and then dried to be weighed for the determination of the residual mass. The weight loss was calculated as the percentage of weight loss by normalizing the sample weight at each time to the initial value. The variation on the samples crystallinity was followed by DSC measurements, meanwhile the sample chemical changes were followed by attenuated total reflectance Fourier transform infrared spectroscopy (ATR-FTIR). The FTIR measurements were conducted at room temperature in transmission mode by a Spectrum One FTIR spectrometer (Perkin Elmer instruments). Spectra were obtained in the 4000-650 cm^{-1} region with a resolution of 4 cm^{-1}.

3. Results and discussions

The morphology of the PU-based nanocomposites was studied by using FE-SEM microscopy, thus analyzing the surface of the transversal section of the cut samples. Fig. 1 collects the images corresponding to the pristine polymer matrix and to the three different processed biodegradable nanocomposites at different magnifications.

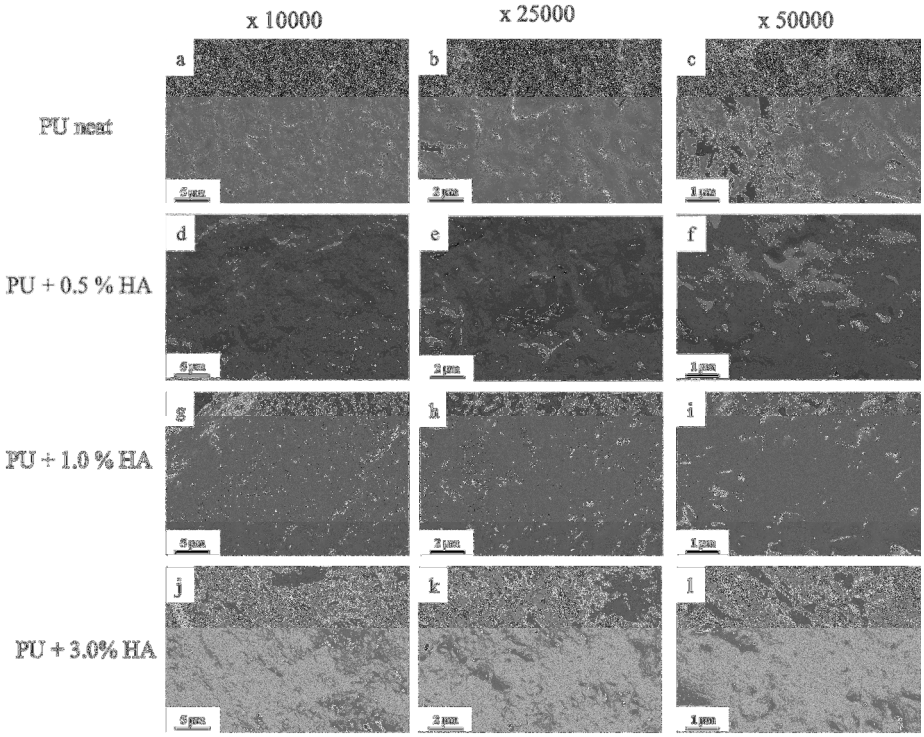

Fig. 1. FE-SEM images corresponding to the nanocomposites of PU with HA at different magnifications: PU neat (a, b, c); PU+0.5% HA (d, e, f); PU+1.0% HA (g, h, i); PU+3.0% HA (j, k, l).

It is worth to note from the FE-SEM images that for all the nanocomposites compositions, the dispersion of the nanofillers into the PU matrix is good. Furthermore, neat PU shows phase separation domains, which have a dimension of about 300 nm and are homogeneously dispersed all over the sample, indicating the segregation of the "hard" and "soft" segments. In particular, the "hard" segments are formed by the PLLA block bonded to the HDI. After the addition of HA nanofillers, the size of the meso-structured domains increases, reaching values of around 800 nm, as it can be better appreciated in the images taken at 50000x of magnification (Fig. 1c, 1f, 1i and 1l). Fig. 2a shows a FE-SEM image of the pristine nHA. Furthermore, TEM analysis has been performed and, as an example, a TEM image for PU+1.0% HA is reported in Fig. 2b.

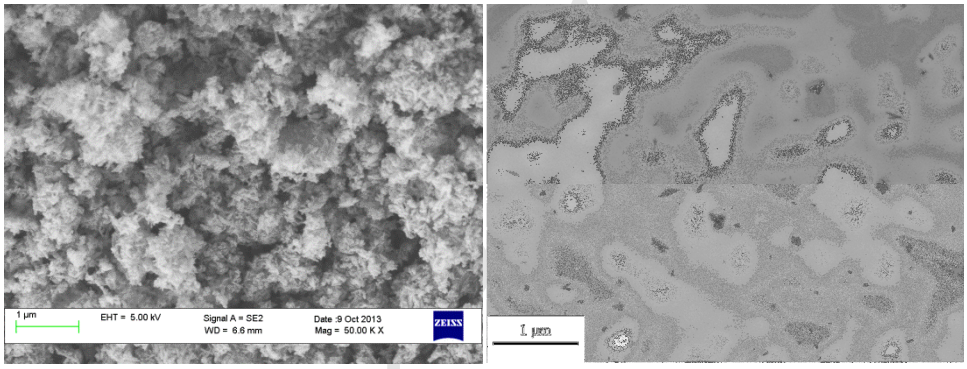

Fig. 2. a) FE-SEM image of the pristine nHA b) TEM image of PU+1.0% HA nanocomposites taken at 75000x.

The TEM image indicates that the HA nanoparticles are well dispersed into the PU matrix.

In order to check the effects of the addition of nHA on the thermal stability of the poly(ester-urethane) and on the thermal degradation mechanism of both PCL and PLLA blocks forming the PU matrix, thermogravimetric analysis has been performed. In Fig. 3 the weight loss profiles (Fig. 3a) and the corresponding derivative curves (Fig. 3b) are shown.

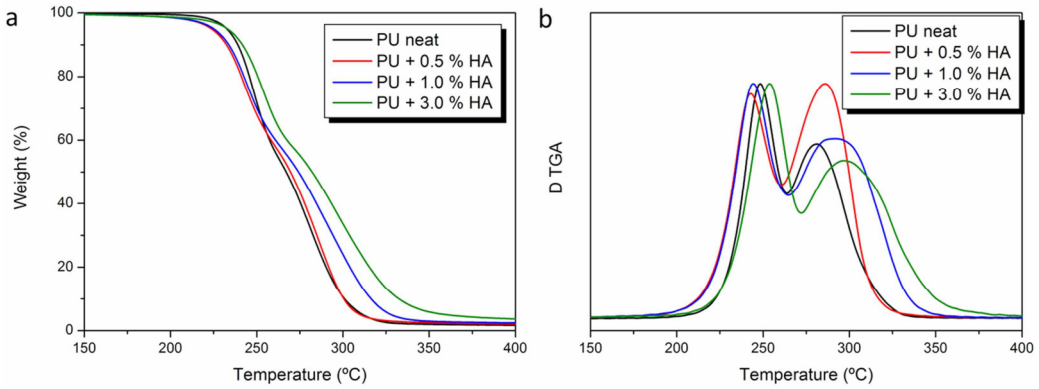

Fig. 3. Thermogravimetric analysis: a) weight loss curves of PU-based nanocomposites reinforced with different HA content. b) derivative curves.

In Fig. 3a it is possible to note that the addition of low amounts of nHA (0.5 and 1 wt %) reduces slowly the thermal stability of the pristine PU, showing an onset temperature of 224 ºC, slightly lower than the initial PU, 232 ºC. On the other hand, with 3 wt % of nHA the onset temperature is about 233 ºC similar to the pure PU. It has been reported by Zhao et al., for contents lower than 4 wt %, nHA is able to increase the thermal stability of polyurethanes and they attributed this behaviour to the formation of hydrogen bonding interactions between hydroxyl groups of nHA and the amide group of polyurethanes [36]. Liu et al. also ascribed the improvements on the thermal stability of polyurethanes loaded with 30 wt % of n-HA to the formation of hydrogen bond interactions [37]. In our case only when 3 wt % nHA has been added, the thermal stability of the PU matrix has been improved. No significant differences were observed by FTIR analysis (not shown) probably due to the low amount of nHA used in the present study. It is well known that the first degradation step of PU corresponds to the degradation of urethane groups [38, 39]. Regarding Fig. 3b, all the materials present two degradation peaks. In order to clarify the effect of nHA in the degradation behavior of the PU matrix, the effect of the different amount of nHA in both the PLLA and PCL phases is discussed separately. In particular, the first degradation peak corresponds to the thermal degradation of the PLLA block with the urethane bond, while the second one, at higher temperature, corresponds to thermal degradation of the PCL block [40]. Consequently, the thermal stability of the poly(ester-urethane) matrix is controlled by the PLLA degradation mechanism. For PLLA it can be observed that the addition of low content (0.5 and 1 wt %) of nHA slightly affects its degradation temperature by

decreasing of about 8 ºC its maximum temperature peak. While, when 3 wt % nHA is added no significantly changes in the degradation peak of PLLA are obtained.

This higher onset degradation temperature of PU+3 HA with respect to the other nanocomposites could be due to the action of the nano-fillers on the mass transport barrier, providing longer paths for the volatile products generated during thermal decomposition to escape, as it was previously suggested by Liu et al. [37].

On the contrary, for all the nanocomposites, the PCL degradation is improved with respect to the neat PU, that is, the degradation peak is shifted from 280 ºC for PCL neat PU to about 300 ºC for the nanocomposites. Moreover, it is easy to note that the higher is the nHA content, the higher is the maximum degradation peak temperature of PCL. In fact, the maximum degradation peak temperature for the PCL block in PU+0.5 HA is about 285 ºC and increases up to 297 ºC for the PCL block in PU+3 HA. This fact indicates that the thermal stability of the PCL block increases with the addition of nHA, attributed to the good affinity of nHA with the PCL-rich phase, probably due to some preference of the free hydroxyl groups of nHA to establish hydrogen bonding interactions with the carbonyl groups of PCL instead of with those of the PLLA. Thus, from TGA results it can be concluded that the addition of HA nanofillers prevents the thermal degradation of the PCL blocks and affects the degradation of the PLLA blocks in the PU-based nanocomposites with low nHA content (0.5 and 1 wt %). It must be underlined that there was no degradation from room temperature to 165 ºC, which is the temperature region where the nanocomposites were processed and/or are intended to be used.

The 1^{st} and 2^{nd} heating DSC scans performed on the nanocomposites are plotted in Fig. **4.** In particular, it is possible to identify the T_m of both PCL and PLLA blocks for all the samples in the first heating (Fig. 4a). The endothermic peak of T_m for the PCL is sharper than the PLLA one, which takes place in a large range of temperatures, from 80 ºC to 140 ºC. On the other hand, in the second heating scans (Fig. 4b) both blocks show cold crystallization process at around 0 ºC for the PCL block and about 50 ºC for PLLA block, respectively, which is overlapped with the melting of the PCL block. Hence, as it occurs for the TGA measurements, the addition of low content nHA slightly affects the thermal behavior of the PLLA block in the nanocomposites. However, when considering the effects of the addition of nHA on the PCL block, it is worth to note that the DSC curves show an increase on the PCL degree of crystallinity for both PU+0.5%

HA and PU+1.0% HA respect to the neat PU, calculated by using the eq. 1. The results obtained from DSC experiments are summarized in Table 1.

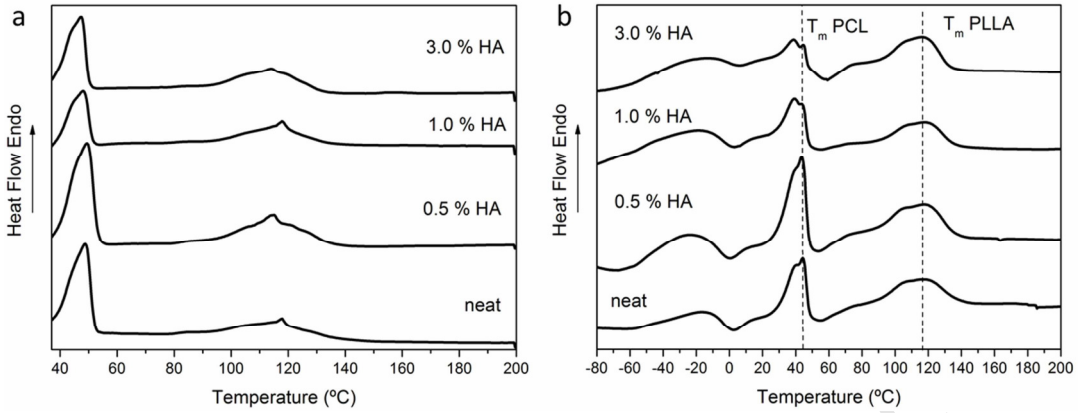

Fig. 4. DSC scans of HA-reinforced nanocomposites: a) 1st heating scans; b) 2nd heating scans.

The T_m of PCL decreases slightly with the addition of nHA while no significant modifications are detected in the T_m of PLLA. The glass transition temperature (T_g), for the PCL block measured at -38.6 ºC for the PU matrix, decreases for all the nanocomposites compositions. In particular, the PU-based nanocomposites reinforced with 1 wt % nHA shows a decrease in the T_g of more than 10 ºC respect to the neat PU.

Table 1. Thermal properties of the PU-based nanocomposites.

Sample	PCL block				PLLA block		
	T_m (ºC)	T_c (ºC)	X_c (%)	T_g (ºC)	T_m (ºC)	T_c (ºC)	X_c (%)
Neat PU	44	-5	9	-39	117	59	34
PU+0.5% HA	44	-2	13	-46	118	59	27
PU+1.0% HA	39	-1	10	-51	118	61	32
PU+3.0% HA	39	-2	7	-43	117	57	33

The T_m of PCL decreases slightly with the addition of nHA while no significant modifications are detected in the T_m of PLLA. The glass transition temperature (T_g), for the PCL block measured at -38.6 ºC for the PU matrix, decreases for all the nanocomposite compositions. In particular, the PU-based nanocomposite reinforced

with 1 wt % nHA shows a decrease in the T_g of more than 10 ºC respect to the neat PU. As occurs with the TGA experiments, these results suggest a preferential interaction of the HA nanofillers with the PCL-rich phase of the PU matrix and that the addition of lower quantities of HA caused a plasticizing effect on the PCL block of the PU matrix. This result can also be correlated with the morphological changes reported in Fig. 1, confirming the interaction of the nHA with the separated PCL-rich phase, which are able to increase their dimension, from 300 to 800 nm when 3 wt % nHA has been added.

Rheological continuous flow experiments have been performed at different temperatures (120, 130 and 140 ºC) in order to study the melt behavior of the nanocomposites (Fig. 5). These temperatures were selected based on the PLLA melting temperature measured by DSC. At 120 ºC (Fig. 5a) a typical non-Newtonian behavior is observed with the viscosity clearly decreasing with the shear rate for each material studied.

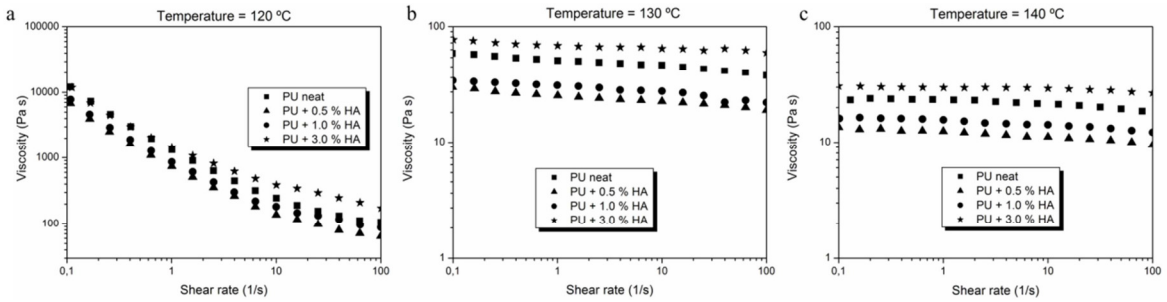

Fig. 5. Rheology of nanocomposites at different temperatures: a) 120 ºC; b) 130 ºC; c) 140 ºC.

On the other hand, at 130 ºC (Fig. 5b) and 140 ºC (Fig. 5c) the viscosity remains quite constant. It is important to note that the addition of nHA at low contents (0.5 and 1 wt % nHA) provokes a decrease in the viscosity compared with the neat polymer matrix at all the studied temperatures. Only PU+3% HA shows a higher value of viscosity than the pure matrix. Hence, at low concentrations the nano hydroxyapatite acts as plasticizer, reducing the viscosity of the system, while by adding 3 wt % nHA the viscosity increases probably due to the hydrogen bonding interactions as a consequence of the higher amount of -OH on the surface of nHA which are able to interact with the polymer matrix. This behavior also agrees well with the reduction of the T_g detected in

DSC measurements. In fact, the smaller is the nHA content, the higher is the reduction of both parameters, T_g and viscosity. The mechanical response of the nanocomposites has been studied by tensile tests. In Fig. 6, the stress-strain curves corresponding to the three different nanocomposites as well as to the neat PU, are reported.

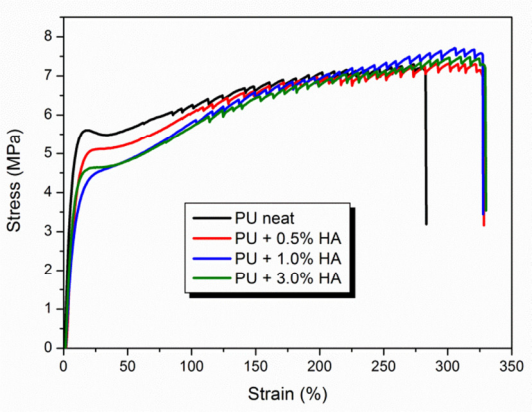

Fig. 6. Stress-strain curves of the HA-reinforced PU-based nanocomposites.

The mechanical properties values have been calculated from the stress-strain curves reported in Fig. 6 and are summarized in Table 2. Due to the addition of nHA the polymer matrix becomes more ductile, reaching higher elongation and maximum strength before break in comparison with the neat matrix. On the contrary, the elastic modulus and the yield stress decrease when the amount of nHA increases. Moreover, as it can be observed in the Fig. 6, the neat PU presents a yield formation that partially disappears after adding the HA nanofillers to the PU matrix. These results are well related with those obtained by rheology and DSC analysis, thus confirming the plasticizing effect of nHA at low content for this polymer matrix. It is also important to note that the standard deviation calculated for all the samples are very small indicating the homogeneity of the nanocomposites and the good dispersion of the nHA into the PU matrix.

Table 2. Mechanical properties and water contact angle measurements of the nHA-reinforced PU-based nanocomposites.

Sample	Elastic modulus (MPa)	Yield stress (MPa)	Maximum stress (MPa)	Elongation at break (%)	WCA (θº)
Neat PU	92.7 ± 9.4	5.52 ± 0.16	7.43 ± 0.18	280 ± 34	67.5 ± 0.9
PU+0.5% HA	70.7 ± 0.2	5.05 ± 0.21	7.32 ± 0.13	317 ± 14	63.4 ± 0.2
PU+1.0% HA	58.6 ± 5.9	4.53 ± 0.08	7.67 ± 0.05	337 ± 16	63.2 ± 0.3
PU+3.0% HA	65.9 ± 7.4	4.52 ± 0.12	7.40 ± 0.12	323 ± 12	61.5 ± 0.3

Studies about the elongation at break with the addition of HA nanoparticles have been reported by other authors. Zhao et al. studied functionalized nHA by introducing isocyanate groups, reporting an increase in elongation at break by increasing the nHA amount [36]. Liu et al. reported an increase in both the elongation and maximum stress when adding 20 and 30 wt % nHA at a polyurethane matrix. In addition, they reported that in concentrations of 40 wt % the influence of nHA agglomerates decrease the elongation at break [37]. It is worth to note that in our nanocomposites, the enhancement in the elongation at break is obtained without functionalizing the nanofillers neither by adding great amounts of nHA.

In Fig. 7, the dynamic mechanical curves for the neat matrix and for the nanocomposite with 3 wt % of hydroxyapatite are reported. The principal thermal transitions were detected for both materials, and they are in good agreement with the previous DSC results. Commonly, the glass transition temperatures for PLLA and PCL are around 60 ºC and -60 ºC, respectively. Regarding the curves of tangent delta, DMA measurements clearly show tan delta peaks at around 0°C and 50°C. (Fig. 7b), thus indicating that both the PCL and PLLA blocks of the poly(ester-urethane) are partially-miscible each other confirming their phase separation, previously reported from FE-SEM images.

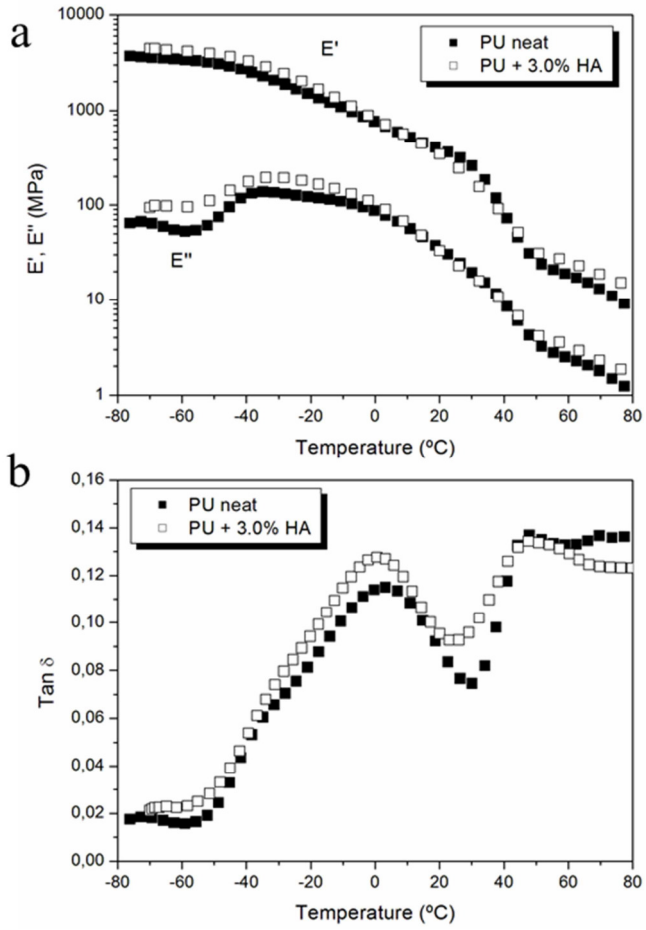

Fig. 7. Dynamic-mechanical behavior of the neat polymer matrix and PU+3.0% HA: a) elastic and loss moduli; b) tan delta.

Moreover, the melting of PCL block is detected, in between 25 ºC and 45 ºC, by a decrease in both moduli and increasing of tangent delta. The addition of nHA does not modify the thermal transitions and provokes a little increase on both moduli respect to the neat matrix, indicating the interaction of the HA nanofiller with the PCL-rich phase; while for the PLLA-rich phase no significant changes are noticed. The results for the other two compositions (0.5 and 1 wt %) show the same trend and they are not shown because they do not provide any additional information.

The surface polarity of PU and PU nanocomposites was studied by means of water contact angle (WCA) measurements (Table 2). Neat PU showed a water contact angle slightly higher than 65º, while the incorporation of nHA decreased the water contact angle values showing values smaller than 65º, typical for hydrophilic surfaces [41]. Thus, the addition of nHA produced more hydrophilic biodegradable nanocomposites

with grater water interaction, required for biomedical applications where the interaction of cells with the material is improved [15, 42].

The in vitro degradation study in PBS has been carried out for a period of five months analyzing a different sample each month. In Fig. 8a the data for the pristine PU matrix and for the nanocomposites with 1 and 3 wt % of nHA are presented. All the materials lost more than 25 wt % after five month of experiment. Regarding the graph, the presence of hydroxyapatite speed up the hydrolytic degradation compared with the PU matrix. This result is in good agreement with surface wettability, since the hydrolytic degradation starts by water absorption followed by the polymer chain broken via ester bonds [42].

DSC measurements were performed to study the change of crystallinity after the degradation experiments, presented in Fig. 8b. The crystallinity of PCL block (filled symbols) increases from values around 20 % to more than 50 % after one month of experiment and until 70 % after five months. For the PLLA blocks (un-filled circles) the crystallinity also is increased, but until lower values, around 40 %. These results suggest that the degradation takes place for the amorphous polymer chains preferentially during the five months of experiment for PCL and for the three months of PLLA degradation. Actually, for PLLA block, the fifth month sample presents lower crystallinity, indicating that also the crystalline PLLA degrades. Lower crystallinity values were reached for the hydroxyapatite reinforced materials.

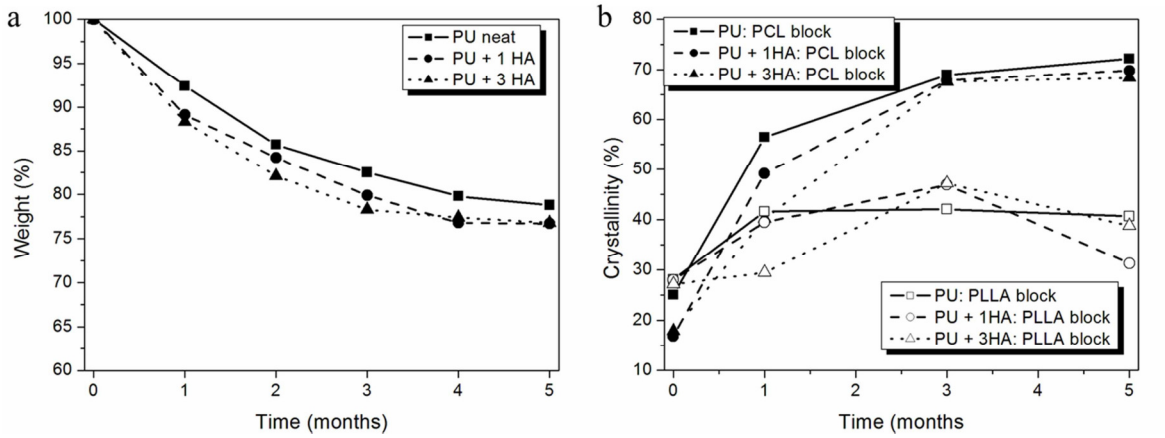

Fig. 8. In vitro degradation results: a) Weight change; b) Crystallinity change of both blocks.

In Fig. 9 the spectra for PU neat at different months of degradations (Fig. 9a) and for the PU+3.0% HA nanocomposite (Fig. 9b) are presented. It is possible to note that the degradation affects the urethane bond (inset of Fig. 9), decreasing the peak intensity at 1536 cm $^{-1}$ which corresponds with the –NH bending [43]. At around 1620 cm^{-1} the appearance of a broad band was observed. This band has been related to the formation of carboxylate ions at the chain ends due to hydrolytic degradation process [44].The same behavior was detected on the hydroxyapatite reinforced nanocomposites, that is, the decrease on the peak associated to urethane bonds and the increase of the band related with carboxylic end groups. No further effects were detected due to the presence of nanofillers in the poly(ester-urethane) during the in vitro degradation.

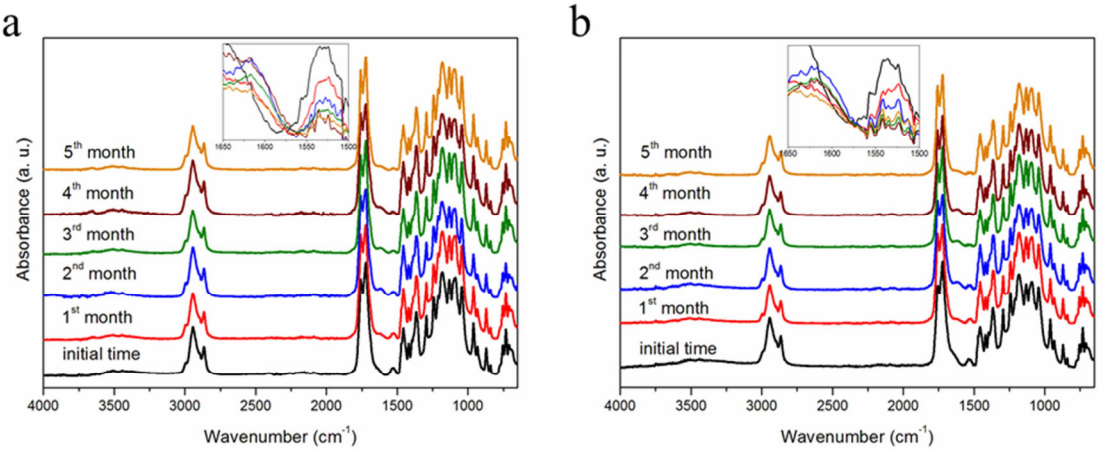

Fig. 9. FT-IR spectra at different degradation times for: a) PU neat; b) nanocomposite PU+3.0% HA.

4. Conclusions

The processing and the characterization in terms of thermal, mechanical, dynamic-mechanical, rheological properties and surface wettability of biodegradable nanocomposites based on poly(ester-urethane) reinforced with nanosized hydroxyapatite obtained by extrusion, with potential biomedical applications, have been reported. FE-SEM images show the effect of the nanofiller on the poly(ester-urethane) morphology, with an increase of the size of the meso-structured domains in the nanocomposites, which is provoked by the interaction of the nanofillers with the separated domains. TEM images have demonstrated the good dispersion of the nHA in the polymer matrices achieved after the processing. The thermal stability of the

poly(ester-urethane) matrix is controlled by the PLLA degradation mechanism. It was observed that the PLLA degradation temperature decreases of about 8 ºC for the low nHA content (0.5 and 1 wt %), while for the nanocomposite with 3 wt % nHA the final thermal stability is not negatively affected. On the contrary, the degradation of the PCL block is prevented by the addition of each of the different amounts of nHA studied. The DSC measurements demonstrate that nHA strongly affects the crystallinity as well as the melting behavior of the PCL block. From these results, it is clear that HA nanofillers interact preferentially with the PCL-rich phase of the polymer matrix, probably due to the formation of hydrogen bonding interactions with the carbonyl groups of PCL with hydroxyl groups of nHA.

The mechanical properties show that the nanocomposites are more ductile than the neat polymer matrix with a slightly decrease of the elastic modulus and the yield stress but with an increment of 115 % in the elongation at break obtained when 3 wt % nHA has been added to the PU matrix. Rheology studies indicate a decrease in the viscosity of the nanocomposites with low nHA content (0.5, 1 wt %). Finally, low amounts of nHA are able to increase the surface water absorption due to the hydrophilic nature of nHA, which increases the wettability of nanocomposite surfaces. From the results obtained by the extensive characterization performed we conclude that at low nanofiller concentration (0.5 and 1 wt %), nHA interacts as plastificant for the poly(ester-urethane) matrix. By increasing the amount of nanofillers, nHA interact also with the urethane bonds due to the hydrogen bonding interactions with the hydroxyl groups of nHA. The in vitro degradation study showed that the presence of nHA allows increasing the nanocomposites degradation rates due to their increased surface hydrophilic character. Therefore, as a general conclusion, two different behaviors have been detected, depending on the amount of nHA, allowing to use the nanofiller as plasticizer for processing (0.5 and 1 wt %), or as reinforcement (3 wt %). These results are very relevant for the processing of poly(ester-urethane)s and in particular for potential application of these nanocomposites in the biomedical sector.

Acknowledgments

We are indebted to the Spanish Ministry of Science and Innovation (MICINN) for their economic support of this research (MAT2013-48059-C2-1-R and MAT2014-55778-REDT) as well as the Regional Government of Madrid (S2013/MIT-2862). LP

acknowledges also, the support of a JAEDoc grant from CSIC cofinanced by FSE. We thank the technical support of Prof. Juan López Martínez from Universitat Politècnica de València (Spain) for his assistance with water contact angle measurements, as well as Marco Rallini and Franco Dominici from the STM group of the University of Perugia for FE-SEM photographs and microextruder blending, respectively.

References

[1] Paul DR, Robeson LM. Polymer nanotechnology: Nanocomposites. Polymer. 2008;49:3187-204.

[2] Rhim JW, Park HM, Ha CS. Bio-nanocomposites for food packaging applications. Prog Polym Sci. 2013;38:1629-52.

[3] Siró I, Plackett D. Microfibrillated cellulose and new nanocomposite materials: A review. Cellulose. 2010;17:459-94.

[4] Azeredo HMCd. Nanocomposites for food packaging applications. Food Res Int. 2009;42:1240-53.

[5] Baur J, Silverman E. Challenges and opportunities in multifunctional nanocomposite structures for aerospace applications. MRS Bull. 2007;32:328-34.

[6] Garcés JM, Moll DJ, Bicerano J, Fibiger R, McLeod DG. Polymeric nanocomposites for automotive applications. Adv Mater. 2000;12:1835-9.

[7] Peponi L, Puglia D, Torre L, Valentini L, Kenny JM. Processing of nanostructured polymers and advanced polymeric based nanocomposites. Mat Sci Eng R. 2014;85:1-46.

[8] Rajesh, Ahuja T, Kumar D. Recent progress in the development of nano-structured conducting polymers/nanocomposites for sensor applications. Sensors Actuat B-Chem. 2009;136:275-86.

[9] Youssef AM. Polymer Nanocomposites as a New Trend for Packaging Applications. Polym-Plast Technol. 2013;52:635-60.

[10] Gibson RF. A review of recent research on mechanics of multifunctional composite materials and structures. Compos Struct. 2010;92:2793-810.

[11] Murugan R, Ramakrishna S. Development of nanocomposites for bone grafting. Compos Sci Technol. 2005;65:2385-406.

[12] Ramakrishna S, Mayer J, Wintermantel E, Leong KW. Biomedical applications of polymer-composite materials: A review. Compos Sci Technol. 2001;61:1189-224.

[13] Ryszkowska JL, Auguścik M, Sheikh A, Boccaccini AR. Biodegradable polyurethane composite scaffolds containing Bioglass® for bone tissue engineering. Compos Sci Technol. 2010;70:1894-908.

[14] Albertsson AC, Varma IK. Recent developments in ring opening polymerization of lactones for biomedical applications. Biomacromolecules. 2003;4:1466-86.

[15] Armentano I, Dottori M, Fortunati E, Mattioli S, Kenny JM. Biodegradable polymer matrix nanocomposites for tissue engineering: A review. Polym Degrad Stab. 2010;95:2126-46.

[16] Ulery BD, Nair LS, Laurencin CT. Biomedical applications of biodegradable polymers. J Polym Sci Pol. 2011;49:832-64.

[17] Vert M, Li SM, Spenlehauer G, Guerin P. Bioresorbability and biocompatibility of aliphatic polyesters. J Mater Sci-Mater M. 1992;3:432-46.

[18] Chen CC, Chueh JY, Tseng H, Huang HM, Lee SY. Preparation and characterization of biodegradable PLA polymeric blends. Biomaterials. 2003;24:1167-73.

[19] Peponi L, Navarro-Baena I, Báez JE, Kenny JM, Marcos-Fernández A. Effect of the molecular weight on the crystallinity of PCL-b-PLLA di-block copolymers. Polymer. 2012;53:4561-8.

[20] Navarro-Baena I, Marcos-Fernández A, Fernández-Torres A, Kenny JM, Peponi L. Synthesis of PLLA-b-PCL-b-PLLA linear tri-block copolymers and their corresponding poly(ester-urethane)s: Effect of the molecular weight on their crystallisation and mechanical properties. RSC Adv. 2014;4:8510-24.

[21] Pan J, Li G, Chen Z, Chen X, Zhu W, Xu K. Alternative block polyurethanes based on poly(3-hydroxybutyrate-co-4-hydroxybutyrate) and poly(ethylene glycol). Biomaterials. 2009;30:2975-84.

[22] Peponi L, Navarro-Baena I, Sonseca A, Gimenez E, Marcos-Fernandez A, Kenny JM. Synthesis and characterization of PCL-PLLA polyurethane with shape memory behavior. Eur Polym J. 2013;49:893-903.

[23] Grande CJ, Torres FG, Gomez CM, Carmen Bañó M. Nanocomposites of bacterial cellulose/hydroxyapatite for biomedical applications. Acta Biomater. 2009;5:1605-15.

[24] Navarro-Baena I, Kenny JM, Peponi L. Thermally-activated shape memory behaviour of bionanocomposites reinforced with cellulose nanocrystals. Cellulose. 2014;21:4231-46.

[25] Mathieu LM, Bourban PE, Månson JAE. Processing of homogeneous ceramic/polymer blends for bioresorbable composites. Compos Sci Technol. 2006;66:1606-14.

[26] Rezwan K, Chen QZ, Blaker JJ, Boccaccini AR. Biodegradable and bioactive porous polymer/inorganic composite scaffolds for bone tissue engineering. Biomaterials. 2006;27:3413-31.

[27] Raksujarit A, Pengpat K, Rujijanagul G, Tunkasiri T. Processing and properties of nanoporous hydroxyapatite ceramics. Mater Design. 2010;31:1658-60.

[28] Laschke MW, Strohe A, Menger MD, Alini M, Eglin D. In vitro and in vivo evaluation of a novel nanosize hydroxyapatite particles/poly(ester-urethane) composite scaffold for bone tissue engineering. Acta Biomater. 2010;6:2020-7.

[29] Kim HW. Biomedical nanocomposites of hydroxyapatite/polycaprolactone obtained by surfactant mediation. J Biomed Mater Res-A. 2007;83:169-77.

[30] Machado HB, Correia RN, Covas JA. Synthesis, extrusion and rheological behaviour of PU/HA composites for biomedical applications. J Mater Sci-Mater M. 2010;21:2057-66.

[31] Dong ZH, Zhang L, Li YB, Zhou G, Lee SW. A guided bone regeneration membrane composed of hydroxyapatite and polyurethane. J Ceram Process Res. 2008;9:478-81.

[32] Khan AS, Ahmed Z, Edirisinghe MJ, Wong FSL, Rehman IU. Preparation and characterization of a novel bioactive restorative composite based on covalently coupled polyurethane-nanohydroxyapatite fibres. Acta Biomater. 2008;4:1275-87.

[33] Kim HW, Lee HH, Knowles JC. Electrospinning biomedical nanocomposite fibers of hydroxyapaite/ poly(lactic acid) for bone regeneration. J Biomed Mater Res-A. 2006;79:643-9.

[34] Sonseca A, Peponi L, Sahuquillo O, Kenny JM, Giménez E. Electrospinning of biodegradable polylactide/hydroxyapatite nanofibers: Study on the morphology, crystallinity structure and thermal stability. Polym Degrad Stab. 2012;97:2052-9.

[35] Fombuena V, Balart J, Boronat T, Sánchez-Nácher L, Garcia-Sanoguera D. Improving mechanical performance of thermoplastic adhesion joints by atmospheric plasma. Mater Design. 2013;47:49-56.

[36] Zhao CX, Zhang WD. Preparation of waterborne polyurethane nanocomposites: Polymerization from functionalized hydroxyapatite. Eur Polym J. 2008;44:1988-95.

[37] Liu H, Zhang L, Li J, Zou Q, Zuo Y, Tian W, et al. Physicochemical and biological properties of nano-hydroxyapatite-reinforced aliphatic polyurethanes membranes. J Biomat Sci-Polym E. 2010;21:1619-36.

[38] Chattopadhyay DK, Webster DC. Thermal stability and flame retardancy of polyurethanes. Prog Polym Sci. 2009;34:1068-133.

[39] Navarro-Baena I, Arrieta MP, Mujica-García A, Sessini V, López D, Kenny JM, et al. Thermal degradation effects on polyurethanes and their nanocomposites. In: Tiwari A, Raj B, editors. Reactions and mechanisms in thermal analysis of advanced materials: Wiley; 2015. p. 165-89.

[40] Navarro-Baena I, Kenny JM, Peponi L. Crystallization and thermal characterization of biodegradable tri-block copolymers and poly(ester-urethane)s based on PCL and PLLA. Polym Degrad Stab. 2014;108:140-50.

[41] Arrieta MP, López J, Hernández A, Rayón E. Ternary PLA-PHB-Limonene blends intended for biodegradable food packaging applications. Eur Polym J. 2014;50:255-70.

[42] Barrioni BR, de Carvalho SM, Oréfice RL, de Oliveira AAR, Pereira MdM. Synthesis and characterization of biodegradable polyurethane films based on HDI with hydrolyzable crosslinked bonds and a homogeneous structure for biomedical applications. Mater Sci Eng C. 2015;52:22-30.

[43] Barrera-Rivera KA, Peponi L, Marcos-Fernández A, Kenny JM, Martínez-Richa A. Synthesis, characterization and hydrolytic degradation of polyester-urethanes obtained by lipase biocatalysis. Polym Degrad Stab. 2014;108:188-94.

[44] Arrieta MP, Fortunati E, Dominici F, Rayón E, López J, Kenny JM. PLA-PHB/cellulose based films: Mechanical, barrier and disintegration properties. Polym Degrad Stab. 2014;107:139-49.

FIGURE CAPTIONS

Fig. 1. FE-SEM images corresponding to the nanocomposites of PU with HA at different magnifications: PU neat (a, b, c); PU+0.5% HA (d, e, f); PU+1.0% HA (g, h, i); PU+3.0% HA (j, k, l).

Fig. 2. a) FE-SEM image of the pristine nHA b) TEM image of PU+1.0% HA nanocomposite taken at 75000x.

Fig. 3. Thermogravimetric analysis: a) weight loss curves of PU-based nanocomposites reinforced with different HA content. b) derivative curves.

Fig. 4. DSC scans of HA-reinforced nanocomposites: a) 1st heating scans; b) 2nd heating scans.

Fig. 5. Rheology of nanocomposites at different temperatures: a) 120 ºC; b) 130 ºC; c) 140 ºC.

Fig. 6. Stress-strain curves of the HA-reinforced PU-based nanocomposites.

Fig. 7. Dynamic-mechanical behavior of the neat polymer matrix and PU+3.0% HA: a) elastic and loss moduli; b) tan delta.

TABLE CAPTIONS

Table 1. Thermal properties of the PU-based nanocomposites.

Table 2. Mechanical properties and water contact angle measurements of the nHA-reinforced PU-based nanocomposites.